Theor Chim Acta (1992) 83: 141–154

Theoretica Chimica Acta

Potential energy surfaces for OsH_2*

Dingguo Dai and K. Balasubramanian**
Department of Chemistry, Arizona State University, Tempe, AZ 85287-1604, USA

Received June 5, 1991/Accepted October 14, 1991

Summary. We compute the potential energy surfaces of 12 electronic states of OsH_2 (four quintet, four triplet, and four singlet) arising from ^5D ground state of the Os atom as well as triplet and singlet excited states using the complete active space multiconfiguration self-consistent field (CAS-MCSCF) followed by multireference configuration interaction (MRCI) and relativistic CI (RCI) calculation which include up to 430,000 configurations. We find that the ^5D ground state of Os atom does not insert into H_2 while the excited ^3F state of Os does. The $^3B_1$ ground state of OsH_2 (there are two other nearly degenerate states) in the absence of spin-orbit coupling was found to be 22 kcal/mol more stable than $Os(^5D) + H_2$. The spin-orbit mixing of $^3B_1$, $^3B_2$, $^3A_2$, and $^1A_1$ states was so strong that it induces significant change in bond angles (up to 10°) for OsH_2.

Key words: Potential energy surfaces – OsH_2 – Relativistic effects

1. Introduction

Transition metal hydrides and dihydrides are interesting from a theoretical standpoint since the nature of metal-hydrogen bonds and the role of metal *d* orbitals are rather intriguing. The potential energy surfaces of transition metal dihydrides could provide significant insight into state specificities of metal-insertion into hydrogen bond. For heavier hydrides, relativistic effects including spin-orbit effects appear to be very significant. It is also important to know if the spin-orbit coupling causes significant contamination of different electronic states which would otherwise not mix nonrelativistically. The role of spin-orbit coupling on the metal atom's reactivity with H_2 is also important to understand.

There have been numerous experimental and theoretical studies on the reactivity of transition metal clusters and atoms and their ions with molecules such as H_2, N_2, CO, etc., in the last few years [1–35]. Such studies appear to have been made with the intent of seeking answers to intriguing questions related

* Dedicated to Prof. Klaus Ruedenberg
** Camille and Henry Dreyfus Teacher-Scholar

to transition metal chemistry and variation of reactivities with cluster size. Such studies have revealed several interesting trends on the reactivity of these species. For example, Smalley and coworkers [2] have studied the reactivity of Co_x, Ni_x, and other clusters with H_2. Beauchamp and coworkers [5, 6], and Armentrout and coworkers [7–10], have studied the reactivity of single transition metal ions with H_2, N_2, D_2, HD, etc., in the gas phase, employing the gas-phase ion beam spectroscopy. Knight and coworkers have made matrix-isolation ESR spectroscopic studies of transition metal dihydride ions such as PdH_2^+ [20].

There have been several theoretical studies on transition metal hydrides and dihydrides [12–35] in recent times. The readers are referred to the recent review by Hay [12] which summarizes the current state of the theoretical developments on not only MH_2 species but also larger organometallic complexes containing W atoms.

One of the authors and Wang studied before the potential energy surfaces of RuH_2 and TcH_2 [34]. It would be interesting to compare and contrast RuH_2 with OsH_2 since the two metal atoms belong to the same group. Indeed we find interesting differences due to large spin-orbit coupling and other relativistic effects of Os which appear to lead to significant differences in the properties of OsH_2 compared to RuH_2.

We obtain the bending potential energy surfaces of 12 electronic states of OsH_2 using the complete active space multiconfiguration self-consistent field (CAS-MCSCF) followed by large scale CI and RCI which included up to 430,000 configurations. An important aspect of our study is the effect of spin-orbit coupling on the electronic states of OsH_2.

2. Method of calculations

The complete active space multiconfiguration self-consistent field (CAS-MCSCF) method was used to generate the entire bending potential energy surfaces of 12 electronic states of OsH_2. Subsequently, higher-order multireference singles + doubles configuration interaction (MRSDCI) calculations were carried out following the CAS-MCSCF, at minima, linear limits and dissociation limits.

All calculations were done using relativistic effective core potentials (RECPs) for the Os atom which retained the outer $5s^25p^65d^66s^2$ shells in the valence space replacing remaining electrons in the relativistic effective core potentials (RECPs). The RECPs of Ross et al. [36] for the Os atom together with the $(5s5p4d)$ valence gaussian basis sets were employed. For the hydrogen atom van Duijneveldt's $(5s1p/3s1p)$ basis set was used.

CAS-MCSCF calculations were made for each electronic state of different spatial symmetry (C_{2v}) and spin multiplicity. For each bending angle (θ), the Os-H bond lengths were optimized using a cubicpolynomial fit and the optimized potential energy surfaces were plotted. The CASSCF active space included four a_1 orbitals, two b_2 orbitals, one b_1 and one a_2 orbitals. Excitations for the $5s^25p^6$ shells of the Os atom were not allowed either at the CASSCF stage or at the CI stage. The saddle points were located as intersections of the potential energy surfaces from the dissociated and linear limits.

Subsequent to CAS-MCSCF, we carry out multireference singles + doubles CI (MRSDCI) calculations. The MRSDCI calculations included single and double excitations from all configurations in the CAS-MCSCF with coefficients $\geqq 0.07$.

The spin-orbit coupling was introduced through the relativistic CI (RCI) method for polyatomics developed by one of the authors [39]. In this method, the spin-orbit integrals are transformed in the MRSDCI natural orbital basis and added to the one-electron CI matrices. The RCI calculations included single and double excitations from all reference configurations which can mix in the C_{2v}^2 double group and which are close in energy.

The low-lying $^3B_1$ state of OsH_2 correlates into A_1, B_2, and A_2 states in the C_{2v}^2 double group. Likewise, $^3A_2$ state splits into A_1, B_1, and B_2 states in C_{2v}^2 while $^3B_2$ state splits into A_1, B_1, and A_2 symmetries. In the RCI of OsH_2, we mix all low-lying states of OsH_2 which have the same symmetry in the C_{2v}^2 double group. For example, our RCI of the A_1 state included leading reference configurations from $^3B_1$, $^3B_2$, $^3A_2$, and several $^1A_1$ states. Table 1 shows the complete list of all reference configurations included in the RCI. For all the reference configurations shown in Table 1, we have included single + double excitations. Consequently, our RCI calculations included the effect of both electron correlation and spin-orbit coupling simultaneously.

All CASSCF/MRSDCI calculations were made using one of the author's [40] modified versions of ALCHEMY II codes [41] to include relativistic effective core potentials. The RCI calculations were made using the general method of RCI for polyatomics described in [42]. The CAS-MCSCF calculations included up to 608 configuration spin functions (CSF) in the C_{2v} symmetry while the MRSDCI method included up to 430,000 CSFs.

Table 1. List of reference configurations of OsH_2 in the RCI

State	Reference configurations
A_1	$1a_1^2 2a_1^2 3a_1 1b_2^2 1b_1 1a_2^2$ (2)
	$1a_1^2 2a_1^2 3a_1^2 1b_2^2 1b_1 1a_2$ (2)
	$1a_1^2 2a_1^2 3a_1 1b_2^2 1b_1^2 1a_2$ (2)
	$1a_1^2 2a_1^2 3a_1^2 1b_2^2 1a_2^2$ (1)
	$1a_1^2 2a_1^2 3a_1^2 1b_2^2 1b_1^2$ (1)
	$1a_1^2 2a_1^2 1b_2^2 1b_1^2 1a_2^2$ (1)
A_2	$1a_1^2 2a_1^2 3a_1 1b_2^2 1b_1 1a_2^2$ (2)
	$1a_1^2 2a_1^2 3a_1^2 1b_2^2 1b_1 1a_2$ (2)
	$1a_1^2 2a_1 3a_1 1b_2^2 1b_1^2 1a_2^2$ (2)
	$1a_1^2 2a_1^2 3a_1 1b_2^2 1b_1^2 1a_2$ (2)
B_2	$1a_1^2 2a_1^2 3a_1 1b_2^2 1b_1 1a_2^2$ (2)
	$1a_1^2 2a_1 3a_1 1b_2^2 1b_1^2 1a_2^2$ (2)
	$1a_1^2 2a_1^2 3a_1 1b_2^2 1b_1^2 1a_2$ (2)
B_1	$1a_1^2 2a_1^2 3a_1 1b_2^2 1b_1^2 1a_2$ (2)
	$1a_1^2 2a_1 3a_1 1b_2^2 1b_1^2 1a_2^2$ (2)
	$1a_1^2 2a_1^2 3a_1^2 1b_2^2 1b_1 1a_2$ (2)

Table 2. Atomic energy separations of Os obtained from asymptotic molecular separations at the dissociation limit

Configuration	Atomic state	E, cm^{-1}	
		Theory	Expt.[a]
$5d^66s^2$	Os(a^5D)	0	0
$5d^7(^4F)6s$	Os(a^3F)	10 930	9 818
$5d^66s^2$	Os(—)[b]	18 905	—

[a] J-weighted average energy separation from [43]
[b] A singlet state of Os from $5d^66s^2$. No experimental atomic data are available on Os singlet states

3. Results and discussion

3.1. Os *atom*

Table 2 compares the asymptotic splitting of molecular states of OsH_2 obtained from our theoretical study with the corresponding experimental values from Moore's tables [43]. We compare the J-weighted experimental values with our values. As seen from Table 2, our computed Os ^3F-^5D energy separation is a bit higher than the experiment. Yet the agreement is ~90%. We find an excited singlet state of Os atom with an energy separation of 18,905 cm^{-1} from the ground state. The electronic configuration of this state is $5d^66s^2$. At the present time, no experimental data exist on excited singlet states of the Os atom and thus this state could not be assigned unambiguously. Note that ^1I, ^1G, ^1F, ^1D, and ^1S states are possible for the $5d^66s^2$ configuration. However, we eliminate the ^1S state as a possibility since more than one singlet state of OsH_2 dissociates into this limit.

3.2. Potential energy surfaces of OsH_2

Figure 1 shows the bending potential energy surfaces of 12 electronic states of OsH_2 (quintet, triplet and singlet). Separate CASSCF calculations were made for each surface in Fig. 1. At each θ, we optimized the Os-H bond lengths and in Fig. 1, we plot the optimized energies. Since these are not state-averaged CASSCF calculations, all electronic states do not exhibit fully accurate asymptotic behavior. Yet most of the electronic states correlate to the correct linear limits and dissociation limits with the exception of the $^3A_1$ state which actually was found to dissociate to a limit slightly higher than Os(^3F) + H_2 at the CASSCF level (hence the dotted line for $^3A_1$ in Fig. 1). However, we believe that invoking state averaging technique would force it to dissociate to the same limit as other triplet states.

One of the most striking features of the potential energy surfaces in Fig. 1 is that the Os(^5D) atom does not insert into H_2. It has surface barriers only a bit below Os(^5D)-Os(^3F) energy separation at the CAS-MCSCF level (Fig. 1). Although these barriers become smaller at the MRSDCI level, it is evident from Fig. 1 that the Os(^5D) atom does not insert into H_2 spontaneously.

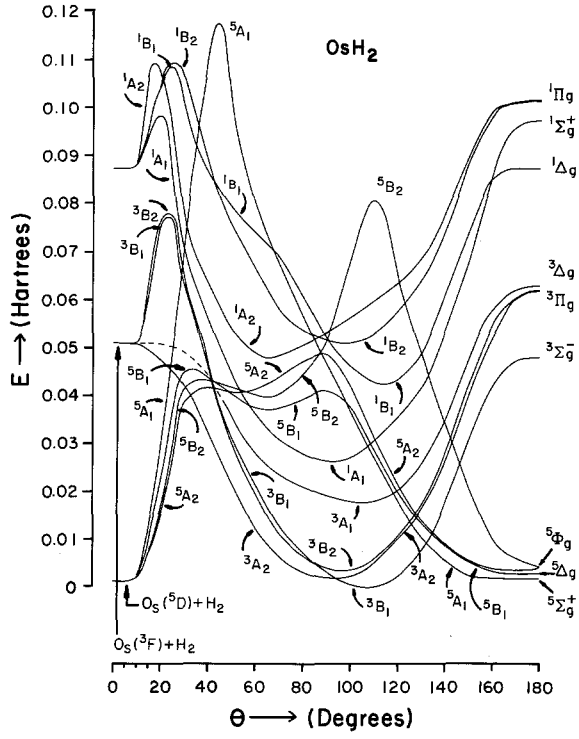

Fig. 1. Bending potential energy surfaces of OsH_2

The $Os(^3F)$ atom, in dramatic contrast to $Os(^5D)$, inserts into H_2 spontaneously at least in two of the available channels to form OsH_2 bent triplet minima. The existence of barriers in the other two channels ($^3B_1$, $^3B_2$) is intriguing but careful analysis of the orbital interaction reveals that $^3A_1$ and $^3A_2$ symmetries are more favorable to minimize repulsive interactions. Furthermore, dissociation of H_2 is achieved primarily through the overlap of the H_2 $1\sigma_u^*$ orbital with $Os(d\pi)$ orbital. Most favorable orbital overlaps are facilitated in $^3A_1$ and $^3A_2$ states.

As evidenced from Fig. 1, the singlet state of the Os atom is more reactive in the $^1A_1$ channel compared to other channels. However, the singlet molecular electronic states are considerably higher than triplet and quintet electric states. Furthermore, the $Os(^5D)$-Os(singlet) energy separation is substantial. Therefore, the formation of several bent singlet minima for OsH_2 is interesting, but the singlet minima are substantially higher.

Some of the saddle points and the shapes of PES (for example $^5B_2$) in Fig. 1 are due to avoided crossings in the wavefunctions which we will discuss in Sect. 4.

3.3. Energy separations of electronic states of OsH_2

At the CASSCF level, the $^3B_1$, $^3A_2$, and $^3B_2$ bent states are almost degenerate with the linear $^5\Sigma_g^+$ and $^5\Delta_g$ states. Hence CASSCF level of theory is not adequate to determine the ground state of OsH_2.

Table 3. Properties of the electronic states of OsH_2 without spin-orbit

State	CASSCF			MRSDCI		
	θ_e, deg	Re, Å	E, eV[a]	θ_e, deg	Re, Å	E, eV[b]
$^3B_1$	108.2	1.628	0.00	95.7	1.593	0.00
$^3A_2$	93.2	1.622	0.05	89.9	1.596	0.37
$^3B_2$	97.5	1.622	0.09	95.1	1.591	0.08
$^3A_1$	105.9	1.639	0.48	103.7	1.601	0.45
$^1A_1$	100.9	1.619	0.72	101.5	1.579	0.73
$^5B_1$	64.4	1.669	1.01	70.5	1.649	0.89
$^5B_2$	65.0	1.661	1.08	68.7	1.631	0.91
$^5A_2$	52.7	1.667	1.11	50.6	1.642	0.92
$^1B_1$	113.8	1.619	1.16	113.8	1.596	1.06
$^1A_2$	67.9	1.597	1.31	61.1	1.556	1.07
$^1B_2$	97.0	1.621	1.39	93.3	1.583	1.16
$^5\Sigma_g^+$	180	1.747	0.05	180	1.735	0.62
$^5\Delta_g$	180	1.765	0.09	180	1.752	0.36
$^5\Phi_g$	180	1.748	0.13	180	1.727	0.17
$^3\Sigma_g^-$	180	1.757	1.32	180	1.733	1.34
$^3\Pi_g$	180	1.746	1.68	180	1.725	1.65
$^3\Delta_g$	180	1.755	1.74	180	1.729	1.68
$^1\Delta_g$	180	1.748	2.39	180	1.726	2.34
$^1\Sigma_g^+$	180	1.742	2.67	180	1.743	2.81
$^1\Pi_g$	180	1.755	2.77	180	1.726	2.69

[a] The zero CASSCF energy is for the $^3B_1$ bent minimum, and is -91.49703 Hartree
[b] The zero MRSDCI energy is for the $^3B_1$ bent minimum, and is -91.59794 Hartree

Table 3 shows the optimized geometries and energy separations in the absence of spin-orbit coupling at the CASSCF and MRCI levels of theory. As seen from Table 3, at the MRCI level of theory the $^3B_1$ state is the ground state while $^3B_2$ is, however, only 0.08 eV above $^3B_1$. Other electronic states of OsH_2 are considerably higher than the $^3B_1$ state except $^5\Phi_g$ which is 0.17 eV above the bent $^3B_1$ state. The near-degeneracy of various triplet states of OsH_2 leads to substantial mixing of these states when spin-orbit coupling is included.

Higher-order electron correlation effects not included in the zeroth-order CASSCF have significant impact on the electronic states of OsH_2 (Table 3). For example the difference between the CASSCF and MRCI θ_es for the $^3B_1$ state is almost 12°. Likewise, the $\Delta\theta_e$ for the $^5B_1$ state due to higher-order electron correlation is $\sim 6°$.

The bond lengths change typically 0.03–0.04 Å due to higher-order correlation effects. The most important impact of electron correlation effects is on energy separation of excited electronic states (Table 3).

As seen from Table 3, the energy separations are so sensitive to higher-order electron correlation effects that the CASSCF and MRSDCI ordering of electronic states differ. For example, at the CASSCF level $^3B_2$ is above $^3A_2$, while at the MRSDCI level the order is reversed. Likewise $^5\Phi_g$ is above $^5\Sigma_g^+$ and $^5\Delta_g$ at the CASSCF while it is below both of these states at the MRCI level.

Table 4 shows the geometries of the saddle points in the potential energy surfaces and the barrier heights relative to the respective dissociation limits.

Table 4. Saddle points in various potential energy curve of OsH_2

State	θ, deg	R, Å	Barrier height, kcal/mol[a]
$^1A_1$	20.4	2.2	7.1
$^1B_1$	24.6	1.9	13.9
$^1B_2$	24.8	2.0	14.0
$^1A_2$	17.3	2.4	14.2
$^3B_1$	22.9	2.1	17.2
$^3B_2$	22.9	2.0	17.3
$^5A_2$	41.0	1.69	25.3
	88.2	1.70	33.1
$^5B_2$	37.8	1.78	26.3
	110.2	1.82	49.9
$^5B_1$	32.0	1.79	27.8
	88.7	1.70	28.0
$^5A_1$	44.1	1.81	86.8

[a] Barrier heights were calculated with respect to the corresponding dissociation limits

Among the quintet states, the smallest barrier is for the $^5A_2$ state which has to surpass a barrier of 25 kcal/mol. Among the triplet states, two surfaces have no barriers while $^3B_1$ and $^3B_2$ states have almost similar saddle points with barriers of 17 kcal/mol. All singlets have saddle points.

The occurrence of multiple saddle points in the $^5A_2$, $^5B_2$, and $^5B_1$ surfaces is quite interesting. These are due to avoided crossings as we discuss in a later section.

3.4. Dissociation energies

Table 5 shows the dissociation energies $D_e(OsH_2)$ relative to $Os(^5D) + H_2$. As seen from Table 5, there is a substantial difference between the CASSCF and

Table 5. Dissociation energies of OsH_2 without spin-orbit effect

State	with respect to $Os(a^5D) + H_2$	
	CASSCF (kcal/mol)	MRSDCI (kcal/mol)
$^3B_1$	0.7	22
$^3A_2$	−0.4	14
$^3B_2$	−1.4	21
$^3A_1$	−10	12
$^1A_1$	−16	6
$^5B_1$	−23	2
$^5B_2$	−24	1
$^5A_2$	−25	1
$^1B_1$	−26	−2
$^1A_2$	−29	−2
$^1B_2$	−31	−4

MRCI values (up to 27 kcal/mol). For example at the MRCI level, the $^3B_1$ ground state is 22 kcal/mol more stable than $Os(^5D) + H_2$, but it is only 0.7 kcal/mol at the CASSCF level.

All triplet states of OsH_2 are stable relative to $Os(^5D) + H_2$ but $^3B_1$ and $^3B_2$ are nearly degenerate in accordance with Table 3. The bent quintet states are only slightly stable compared to $Os(^5D) + H_2$ but the linear electronic states exhibit enhanced stabilities for the qunitet manifold of electronic states. Due to the crossing of triplet and quintet states in Fig. 1, the nonadiabatic effects would predissociate all triplet electronic states into $Os(^5D) + H_2$. Consequently, the dissociation energies are reported relative to $Os(^5D) + H_2$.

Benavides-Garcia and Balasubramanian [44] have computed the spectroscopic constants and potential energy curves for 21 electronic states of OsH including spin-orbit coupling. They computed the D_e of OsH as 2.32 eV. From this and $D_e(H_2)$, we deduce the stability of OsH_2 relative to OsH + H as 3.1 eV.

3.5. Spin-orbit effects

Table 6 shows the geometries and RCI compositions of electronic states of OsH_2 when spin-orbit effects are included. The most notable features of the spin-orbit states are that they are strongly mixed in character. For example, the $A_1(I)$ spin-orbit component is 52% $^3B_1$ and 43% $^3B_2$. This is due to the near-degeneracy of $^3B_1$ and $^3B_2$ states (see Table 3). However, since the geometries of the two states are similar there is no substantial change in the bond angles of the $A_1(I)$ component.

In general, the changes in the geometries of the spin-orbit components of OsH_2 are determined by the corresponding states which are heavily mixed. For example, the $A_1(II)$ state undergoes significant geometry change compared to the primary contribution ($^3A_2$) due to large mixing with $^3B_1$ and $^3B_2$ states. Consequently, the $^3A_2$ states experience a H$\diagup^{Os}\diagdown$H bond angle increase of $\sim 10°$.

The spin-orbit coupling removes the near-degeneracy of $^3B_1$ and $^3B_2$ states in the sense $A_1(I) - A_1(II)$ splitting is 0.30 eV. However, it introduces new degeneracy since the A_1 and A_2 spin-orbit components of ($^3B_1$, $^3B_2$) mixture are nearly degenerate. Hence spin-orbit effects are significant for OsH_2 and have interesting impact on the geometries and energy separation.

Table 6. Properties of the bent states of OsH_2 including spin-orbit effect

Relativistic state	θ_e, deg	R_e, Å	E, eV	Weight in percent
$A_1(I)$	100.0	1.606	0.00	52% $^3B_1$, 43% $^3B_2$, 3% $^1A_1$, 0.2% $^3A_2$
$A_2(I)$	99.3	1.605	0.01	51% $^3B_1$, 45% $^3B_2$, 2% $^1A_2$
B_1	89.9	1.598	0.21	59% $^3B_2$, 40% $^3A_2$, 0.01% $^3A_1$
$B_2(I)$	103.3	1.605	0.29	89% $^3B_1$, 10% $^3A_2$
$A_1(II)$	99.7	1.607	0.30	42% $^3A_2$, 22% $^3B_1$, 22% $^3B_2$, 12% $^1A_1$
$A_2(II)$	100.7	1.601	0.66	51% $^3B_2$, 48% $^3B_1$, 0.1% $^1A_2$
$B_2(II)$	96.6	1.604	0.86	86% $^3A_2$, 12% $^3B_1$, 0.1% $^3A_1$
$A_1(III)$	102.5	1.607	1.73	81% $^1A_1$, 14% $^3A_2$, 2% $^3B_1$, 0.2% $^3B_2$

Table 7. Dipole moment for the bent minimum of OsH_2

State	μ, D[a]
$^3B_1$	2.43
$^3A_2$	2.77
$^3B_2$	2.25
$^3A_1$	2.21
$^1A_1$	2.13
$^5B_1$	−0.08
$^5B_2$	−0.02
$^5A_2$	−0.49
$^1B_1$	1.69
$^1A_2$	2.22
$^1B_2$	2.22

[a] Polarity is Os^+H^-

3.6. Dipole moments

Table 7 shows the dipole moments of the bent electronic states of OsH_2. With the exception of quintet bent minima, all triplet and singlet states exhibit considerable change transfer from Os to H atoms resulting in Os^+H^- polarities of bonds. This is consistent with electron-rich metallic character of the Os atom. The quintet states have vanishingly small dipole moments as they form small angle minima. The negative dipole moment of $^5A_2$ is interesting as this is suggestive of exchange of electronic density from hydrogen to Os. This is consistent with small angle (acute) minima which are facilitated by exchange of electric density from hydrogens to vacant Os orbitals in quintet states.

4. The nature of electronic states of OsH_2

Table 8 shows the leading configurations in the MRSDCI wavefunction of the bent electronic states of OsH_2. As seen from Table 8, the high-spin states (all triplet and quintet) are relatively simple in that they are well represented by their leading (single) configurations. Also with the exception of the $^1A_1$ state, all singlet states of OsH_2 are simple, too. Only the $^1A_1$ state of OsH_2 is quite complex in its character.

The double hump in the potential energy surfaces of $^5B_1$, $^5B_2$, and $^5A_2$ (Fig. 1) is due to avoided crossings. For $\theta < 20°$, the $^5B_1$ state is predominantly composed of $1a_1^2 2a_1^2 3a_1 4a_1 1b_2 1b_1^2 1a_2$ (coefficient is 0.994) while for $\theta = 50°-80°$, it is mainly composed of $1a_1^2 2a_1 3a_1 4a_1 1b_2^2 1b_1 1a_2^2$ (0.976). At $\theta = 90°$, it is made of $1a_1^2 2a_1 3a_1 1b_2^2 2b_2 1b_1^2 1a_2$ (0.981). These avoided crossings in the $^5B_1$ state result in the double hump potential surface in Fig. 1.

The $^5B_2$ state is predominantly $1a_1^2 2a_1 3a_1^2 4a_1 1b_2^2 1b_1 1a_2$ (0.994) for $\theta < 30°$ while for $\theta = 50°-90°$, it is composed of $1a_1^2 2a_1^2 3a_1 4a_1 1b_2^2 1b_1 1a_2$ (0.976). At $\theta = 130°$ it is mainly composed of $1a_1^2 2a_1 3a_1 1b_2^2 2b_2^2 1b_1 1a_2$ (0.989). Hence the double hump in the $^5B_2$ bending surface is due to these avoided crossings.

Table 8. Leading configurations in the MRSDCI of the bent states of OsH_2

State	Coefficient	Configuration							
		$1a_1$	$2a_1$	$3a_1$	$4a_1$	$1b_2$	$2b_2$	$1b_1$	$1a_2$
$^3B_1$	−0.950	2	2	1	0	2	0	1	2
$^3A_2$	0.956	2	2	1	0	2	0	2	1
$^3B_2$	0.950	2	2	2	0	2	0	1	1
$^3A_1$	0.948	2	1	1	0	2	0	2	2
$^1A_1$	−0.518	2	2	0	0	2	0	2	2
	−0.516	2	2	2	0	2	0	0	2
	0.479	2	0	2	0	2	0	2	2
	0.388	2	2	2	0	2	0	2	0
$^5B_1$	0.948	2	1	1	1	2	0	1	2
$^5B_2$	0.949	2	2	1	1	2	0	1	1
$^5A_2$	−0.916	2	1	1	1	2	0	2	1
$^1B_1$	0.950	2	2	1	0	2	0	1	2
$^1A_2$	0.948	2	2	1	0	2	0	2	1
$^1B_2$	0.942	2	2	2	0	2	0	1	1

Similarly, the $^5A_2$ state is predominantly $1a_1^2 2a_1^2 3a_1 4a_1 1b_2 1b_1 1a_2^2$ (0.994) for $\theta < 30°$ while at $\theta = 70°$, it is made of $1a_1^2 2a_1 3a_1 4a_1 1b_2^2 1b_1^2 1a_2$ (0.974). At $\theta = 90°$, it is mainly composed of $1a_1^2 2a_1 3a_1 1b_2^2 2b_2 1b_1 1a_2^2$ (0.982).

Table 9 shows the composition of the linear electronic states. The high-spin quintet electronic states are simpler in character in that they are described by their leading configurations. All triplet and singlet states are noticeably complex in their overall compositions.

Table 10 shows the Mulliken population analysis for the electronic states of OsH_2. As seen from this table the ground state Os population is $5d^{6.9}6s^{0.8}6p^{0.2}$. There is some $5d^7 6s^1$ and $5d^6 6s^2$ mixing in the ground state of OsH_2. However, the population is closer to $5d^7 6s^1$ atomic configuration. This is expected since a pure $5d^6 6s^2$ configuration cannot form very stable Os-H bonds due to filled $6s$ shells. The formation of the Os-H bonds is facilitated through the promotion of one of the $6s$ electrons to Os $5d$. The overall Os total populations (except $^1A_2$) are less than 8.0 indicating transfer of electronic density from Os to H atoms.a

5. Comparison of OsH_2 with RuH_2

There are a number of differences and similarities between OsH_2 and RuH_2. Balasubramanian and Wang [34] have computed the potential energy surfaces of RuH_2. There are two nearly-degenerate candidates for the ground states of RuH_2 namely $^3A_2$ and $^3B_1$. The $^3B_2$ electronic state of RuH_2 is only 0.27 eV above the $^3A_2$ minimum for RuH_2. The θ_e values for the $^3A_2$, $^3B_1$, and $^3B_2$ states of RuH_2 are 73°, 99°, and 86°, respectively, while the corresponding θ_es for OsH_2 are 90°, 95.7°, 95.1°, respectively. The differences in the bond angles arise from the differences in hybridization, which are in turn due to relativistic effects.

Table 9. Important configurations in the MRSDCI of the linear states of OsH_2

State	Coefficients	Configuration						
		$1\sigma_g$	$2\sigma_g$	$3\sigma_g$	σ_u	δ_g	π_g	π_u
$^5\Sigma_g^+$	0.992	2	0	0	2	2	2	2
$^5\Delta_g$	−0.991	2	1	0	2	3	2	0
$^5\Phi_g$	−0.992	2	1	1	2	1	3	0
$^3\Sigma_g^-$	0.581	2	0	0	2	4	2	0
	−0.437, −0.437	2	2	0	2	2	2	0
	−0.246	2	1	0	2	3	2	0
$^3\Pi_g$	−0.701	2	1	0	2	2	3	0
	0.422, −0.272	2	1	1	2	1	3	0
	0.403	2	2	1	2	0	3	0
$^3\Delta_g$	0.753, −0.508	2	1	0	2	3	2	0
	0.244	2	2	0	2	2	2	0
$^1\Delta_g$	−0.656	2	1	0	2	3	2	0
	0.516	2	0	0	2	4	2	0
	−0.409	2	2	0	2	2	2	0
$^1\Sigma_g^+$	0.654, 0.222	2	1	0	2	1	2	2
	−0.458, 0.187	2	0	0	2	2	2	2
	−0.381, 0.344	2	2	0	2	0	2	2
$^1\Pi_g$	0.589	2	1	0	2	2	3	0
	0.392	2	1	1	2	1	3	0
	0.385	2	2	0	2	1	3	0
	0.383	2	2	1	2	0	3	0
	−0.336	2	2	1	2	2	1	0

Table 10. Mulliken population analysis for the electronic states of OsH_2

State	Gross population[a]					Overlap
	Os	H	Os(*s*)	Os(*p*)	Os(*d*)	
$^3B_1$	7.924	2.076	0.802	0.186	6.936	1.142
$^3A_2$	7.929	2.071	0.889	0.168	6.871	1.157
$^3B_2$	7.927	2.073	1.263	0.175	6.489	2.034
$^3A_1$	7.890	2.110	0.678	0.180	7.032	2.070
$^1A_1$	7.914	2.086	1.139	0.186	6.588	1.158
$^5B_1$	7.852	2.148	0.880	0.610	6.363	0.831
$^5B_2$	7.883	2.117	0.873	0.642	6.368	0.883
$^5A_2$	7.904	2.096	0.930	0.509	6.465	0.505
$^1B_1$	7.906	2.094	0.945	0.207	6.754	1.151
$^1A_2$	8.034	1.966	1.053	0.167	6.815	1.030
$^1B_2$	7.945	2.055	1.289	0.190	6.466	2.106

[a] We omit the $5s^25p^6$ shells of Os in this table

The differences between RuH_2 and OsH_2 are mainly due to relativistic mass-velocity and spin-orbit effects. Due to the large relatively mass-velocity contraction, the 6*s* orbital is stabilized. This leads to a $5d^6 6s^2(^5D)$ ground state for the Os atom while the ground state of the Ru atom is $4d^7 5s^1(^5F)$. This combined with the fact that spin-orbit effects are significantly larger for Os leads to dramatic differences in both the hybridizations and reactivity patterns.

The $Os(5d^6 6s^2; {}^5D) - Os(5d^7 6s^1; {}^3F)$ energy separation is substantially higher ($9878\,cm^{-1}$) compared to $Ru(4d^7 5s^1; {}^5F) - Ru(4d^7 5s^1; {}^3F)$ energy separation ($6308\,cm^{-1}$) [40]. The barrier that the $Ru({}^5F)$ atom has to surpass is only 9 kcal/mol at the MRSDCI level in the $^5B_1$ channel mainly because the $Ru(4a^7 5s^1)$ atom is more reactive than $Os(5d^6 s^2)$. The barrier that Os atom has to surmount is considerably larger ($\sim$25 kcal/mol).

A striking contrast between RuH_2 and OsH_2 is that RuH_2 forms only linear minima in the quintet surfaces while OsH_2 exhibits acute angle minima. The main reason for this difference is because of the difference in the electronic configurations of the quintet states of the two atoms (Os: $5d^6 6s^2$, Ru $4d^7 5s^1$), which is in turn due to relativistic effects. The vacant 6*p* orbital of Os atom is slightly lower and can thus accept electronic density from hydrogen atoms. An effective 5*d*6*s*6*p* hybridization in this region leads to the acute angle structures for OsH_2 (see Table 10).

The OsH_2 ground state is $\sim$22 kcal/mol more stable compared to $Os({}^5D) + H_2$ while RuH_2 $^3B_1$ ground state is $\sim$16 kcal/mol more stable than $Ru({}^5F) + H_2$. The spin-orbit effects are significantly larger for OsH_2 and are expected to introduce some destabilization of OsH_2 molecular states relative to $Os + H_2$. Consequently, the stabilities of molecular states of OsH_2 are enhanced compared to RuH_2.

In general OsH_2 electronic states exhibit enhanced 6*s* character while the RuH_2 electric states exhibit enhanced 4*d* character. This is due to relativistic stabilization of the 6*s* orbital of Os discussed before. For example, in the $^3B_1$ state of RuH_2, the Ru atom has $4d^{7.2}5s^{0.6}5p^{0.15}$ Mulliken populations while Os atom has $5d^{6.9}6s^{0.8}6p^{0.2}$ population. This difference in the hybridization leads to the difference in the bond angles on the two molecules. The Ru-H overlaps of all triplet and singlet electronic states are near 1.2–1.25. The Os-H overlaps are, however, significantly larger suggesting stronger Os-H bonds compared to Ru-H bonds. The dipole moments of both the molecules are comparable and suggest significant M^+H^- polarities.

6. Conclusion

In this paper we studied the potential energy surfaces of 12 electronic states of OsH_2 using CASSCF/MRSDCI levels of theory. We found that the $Os(5d^6 6s^2; {}^5D)$ atom does not insert into H_2 while the excited $Os(5d^7 6s^1; {}^3F)$ atom inserts into H_2. Two nearly degenerate bent electronic states of $OsH_2({}^3B_1, {}^3B_2)$ were found as candidates for the ground states of OsH_2 at the MRSDCI level. The spin-orbit coupling among the nearly-degenerate states of OsH_2 was found to be so strong that the $A_1(I)$ spin-orbit state of OsH_2 was found to be 52% $^3B_1$ and 43% $^3B_2$. The spin-orbit coupling was shown to change bond angle by almost 10°. The analyses of the electronic states revealed considerable 5*d*6*s*6*p* hybridization in the bent quintet minima while the triplet states have much smaller 6*p* character. The Os-H bonds were found to exhibit Os^+H^- polarities consistent with computed dipole moments.

Acknowledgements. This research was supported by US Department of Energy under grant DEFG0286ER13558. Dingguo Dai thanks the Department of Chemistry, Tongji University, Shanghai, People's Republic of China, for providing a leave which made this joint study possible.

References

1. Collman JP (1968) Acc Chem Res 1:169
2. Smalley RE (1985) in: Bartlett RJ (ed) Comparison of *ab initio* quantum chemistry with experiment. Reidel, NY, p 53
3. Crabtree RH (1985) Chem Rev 85:245; Crabtree RH (1990) Acc Chem Res 23:95
4. Kubas GJ (1988) Acc Chem Res 21:120
5. Armentrout PB, Beauchamp JL (1989) Acc Chem Res 22:315
6. Martinho JA, Beauchamp JL (1990) Chem Review 90:629
7. Armentrout PB, Halle LF, Beauchamp IL (1981) J Am Chem Soc 103:6501
8. Elkind JL, Armentrout PB (1986) Inorg Chem 25:1078; (1986) J Phys Chem 96:5736, 651
9. Sunderlin LS, Armentrout PB (1989) J Am Chem Soc 111:3458
10. Elkind JL, Sunderlin LS, Armentrout PB (1989) J Phys Chem 92:3151
11. Hanton, SD, Noll RJ, Weisshaar JC (1990) J Phys Chem 94:3654; Sanders L, Hanton SD, Weisshaar JC (1990) J Phys Chem 92:3498
12. Hay PJ (1991) in: Dedieu A (ed) Transition metal hydrides, VCH, NY
13. Balasubramanian K, Ravimohan Ch (1989) J Phys Chem 93:4490
14. Balasubramanian K, Liao DW (1988) J Phys Chem 92:6259
15. Balasubramanian K, Liao MZ (1988) J Phys Chem 92:361
16. Rappe AK, Upton TH (1986) J Chem Phys 85:4400
17. Elkind JL, Armentrout PB (1986) J Phys Chem 91:2037
18. Sanders L, Hanton S, Weisshaar JC (1987) J Phys Chem 91:5145
19. Schilling JB, Goddard III, WA, Beauchamp JL (1986) J Am Chem 108:582; (1987) 109:5565
20. Knight Jr LB, Cobranchi ST, Herlong J, Kirk T, Blasubramanian K, Das KK (1990) J Chem Phys 92:2721
21. Das KK, Balasubramanian K (1990) J Chem Phys 92:6697
22. Balasubramanian K, Liao DW (1988) J Phys Chem 92:6259
23. Hay PJ (1990) J Am Chem Soc 112:2324; Noell O, Hay PJ (1984) J Am Chem Soc 106:6928; Hay PJ (1987) J Am Chem Soc 109:705
24. Alvarado-Swaisgood AE, Harrison JF (1985) J Phys Chem 89:5198; Alvarado-Swaisgood AE, Allison A, Harrison JF (1985) J Phys Chem 89:2517; Rivera M, Harrison JF, Alvarado-Swaisgood (1990) J Phys Chem 94:6979
25. Aglada J, Bruna DJ, Peyerimhoff SD, Buenker RJ (1988) J Mol Spectr 93:299
26. Rivera M, Harrison JF, Alvarado-Swaisgood A (1990) J Phys Chem 94:6969; Mavridis M, Harrison JF (1989) J Chem Soc Faraday, Trans 2 85:1391
27. Balasubramanian K (1988) Int J Quantum Chem Symp S22:319
28. Trinquier G, Hoffmann R (1984) Organometallics 3:370
29. Blomberg MRA, Siegbahn PEM (1983) J Chem Phys 78:986, 5682
30. Low JJ, Goddard III WA (1986) J Am Chem Soc 108:6115; Low JJ, Goddard III WA (1986) Organometallics 5:609
31. Li JQ, Balasubramanian K (1990) J Phys Chem 94:545
32. Das KK, Balasubramanian K (1989) J Chem Phys 91:6254
33. Rao BK, Khanna SN, Jena P (1991) Phys Rev B 43:1416
34. Balasubramanian K, Wang JZ (1989) J Chem Phys 91:7761
35. Poulain E, Novaro O, Ruiz ME (1990) J Mol Structure (Theochem) 69:337
36. Desclaux JP, Pyykkö P (1976) Chem Phys Lett 39:300
37. Desclaux JP, Pyykkö P (1974) Chem Phys Lett 29:534
38. Schwerdtfeger P, Dolg M, Schwarz WHE, Bownmaker GA, Boyd PW (1989) J Chem Phys 91:1762

39. Ross RB, Powers JM, Atashroo T, Ermler WC, LaJohn LA, Christiansen PA (1990) J Chem Phys 93:6654
40. Balasubramanian K (1986) Chem Phys Lett 127:585
41. The major authors of ALCHEMY II codes are Liu B, Yoshimine M, Lengsfield B
42. Balasubramanian K (1988) J Chem Phys 89:5731
43. Moore CE (1981) Atomic energy levels (National Bureau of Standards, Washington), Vol 2
44. Benavides-Garcia M, Balasubramanian K (1991) J Mol Spectr 150:271